Journal of Mines, Metals and Fuels, *73(7): 2095-2107; 2025. DOI: 10.18311/jmmf/2025/49192*

Print ISSN : 0022-2755

Journal of Mines, Metals and Fuels

Contents available at: *www.informaticsjournals.co.in/index.php/jmmf*

A Compact Arrowhead-Shaped Feed Circular Metallic Microstrip Patch Triple-Band Antenna for Multi-Standard Wireless Communication Services

Pawan D. Kale[1,2]*, Santosh B. Patil[1], Dhiraj P. Tulaskar[1], Vishal Bhope[2], Disha Parkhi[2], and Tushar Dadasaheb Gadekar[3]

[1]Department of Electronics and Telecommunication Engineering, Shri Sant Gajanan Maharaj College of Engineering, Shegaon - 444203, Maharashtra, India; kalepawan21@gmail.com

[2]Department of Electronics and Telecommunication Engineering, Marathwada Mitra Mandal's College of Engineering, Pune - 411052, Maharashtra, India

[3]Department of Mechanical Engineering, Marathwada Mitra Mandal's College of Engineering, Pune - 411052, Maharashtra, India

Abstract

This manuscript expounds on designing and analysing a compact triple-band microstrip antenna optimised for multi-standard wireless communication services. The antenna initially exhibits dual resonant modes by introducing a semicircular arch-shaped structure around a circular ring with an arrowhead-shaped feed. Incorporation of the plano-convex ground plane with a triangular defect adds a third band with better impedance matching and enhances the broader bandwidth of 1.39 GHz at the second frequency band. The projected antenna structure is designed to operate on triple resonant frequencies suitable for multi-standard wireless services such as Wireless Local Area Network (WLAN) (2.4/5.2 GHz), Worldwide Interoperability for Microwave Access (WIMAX) (2.5/3.5 GHz), and the 5th Generation (5G) New Radio (NR) Sub-6 GHz band (n78 band and n79 band). The frequency of operation is taken as 2.4, 4.2, and 5.2 GHz, resonating within the band of 2.33-2.64 GHz, 3.57-4.96 GHz, and 5.08-5.37 GHz. The fabricated device measuring just 36×25 mm^2 uses Flame Retardant 4 (FR4) epoxy material as a substrate. The performance of the projected triple-band antenna has been achieved by utilising the Advanced Design System (ADS) software. The optimised antenna structure effectively balances compactness with superior impedance matching, achieving a Return Loss (S11) of -13.59, -29.70, and -17.91 db and a Voltage Standing Wave Ratio (VSWR) < 2 at the three resonant frequencies. The proposed design attains bandwidths of 310, 1390, and 290 MHz and a gain of 2.92, 3.76, and 4.24 dBi while ensuring a uniform radiation pattern, hence making it a strong candidate for next-generation wireless communication services.

Major Findings: *The proposed tri-band antenna achieves resonance at three distinct frequency bands with superior impedance matching and stable radiation patterns. The compact design offers enhanced bandwidth and gain, making it suitable for WLAN, WIMAX, and 5G communication.*

Keywords: *5G Bands, Defected Ground Plane (DGP), Microstrip Patch Antenna (MPA), Triple Band Antenna, WIMAX, WLAN*

**Author for correspondence*

1.0 Introduction

Advancements in wireless communication require miniaturised devices that are capable of maintaining high-quality connectivity. Antennas play a crucial role in attaining such connectivity. About wireless communication, the miniaturisation of the antenna usually impacts the gain and bandwidth. The balance between achieving miniaturisation and encountering larger performance trade-offs has been the focus of many recent studies[1-3]. The antenna is made out of a dielectric substrate with a radiating metallic patch, where patch dimensions and dielectric properties determine its resonant frequency[4,5]. By adjusting these features, multiple resonant modes are achieved for operation across different spectrums. Benefits include compact size, high efficiency, and broad bandwidth, allowing for integration into portable electronics such as smartphones[6]. The wide bandwidth capability is vital for systems needing high-data transfer rates and adaptability despite interference. However, challenges arise in achieving effective impedance matching across numerous bands, complicating the alignment between the antenna and transmission line as operational bands increase[7]. The design process is complex, requiring advanced simulation for optimizing patch dimensions and precise fabrication techniques. These antennas are widely used for multi-standard services like WLAN, WIMAX, and emerging 5G technology, each with unique design needs[8].

The literature reveals a progression of innovative designs aimed at miniaturisation, enhancing the bandwidth, impedance matching, gain, and overall efficiency of the antenna while addressing the challenges presented by various frequency bands. In recent years, various shapes of MPA have been investigated to improve the antenna's performance. Paper[9] presents a compact Asymmetric Coplanar Strip (ACS)-fed triple-band antenna for WLAN and WIMAX, using J-shaped and open stub arms. The ACS-fed structure may introduce fabrication complexity. A multiband monopole antenna with an S-shaped strip and a notched rectangular loop was proposed in[10], achieving triple resonance with bandwidth enhancement. The design is compact, but integrating multilayer circuits may be challenging due to the ground slot. The author in[11] develops a rectangular antenna with notches and slots for triple band operation. It is effective for Bluetooth and L-band applications, but the lower frequency operation increases the patch size. Article[12] introduces a rupee-shaped tri-band Coplanar Waveguide (CPW)-fed MPA. Its small size is beneficial, but the CPW-fed structure may complicate fabrication. MPA presents a cost-effective, easily integrated solution for WLAN and WIMAX, functioning in 2.4 GHz and 5 GHz bands while accommodating wide bandwidths and polarization diversity, vital for sustaining reliable connections amongst variable interference[13]. Features like effective impedance matching and low cross-polarization help reduce interference and improve system performance. Kumar and Srivastava in[1] explored the bandwidth characteristics of rectangular and circular patch antennas on thick substrates. Their findings indicated that theoretical bandwidth results were inferior to simulated outcomes, underscoring the need for effective techniques in antenna analysis and design to optimise performance. Elkorany *et al.* in[14] design a tri-band antenna using two F-shaped resonators and a truncated patch for wireless sensor and mobile applications. It achieved peak gains of 5.2 db. Its relatively large size (60×50 mm^2) may not be ideal for compact devices. Karthikeyan M *et al.* in[15] presents a stacked T-shaped strip antenna with a DGP and achieved a maximum bandwidth of 1.52 GHz at the 3rd band. Paper[16] presents a compact antenna for WLAN and WIMAX applications, incorporating rectangular slotting in the ground plane and a fork-shaped strip in a modified rectangular ring to achieve tri-band operation. The antenna demonstrates a peak gain of 4.76 dBi and radiation efficiencies of 87.6%. A triple-band patch antenna using meander lines for resonance control is proposed in the paper[17]. It features a compact, low-cost design with stable impedance bandwidths, making it suitable for wireless communication systems. However, the design has narrow bandwidth and limited gain, which may restrict its performance in high data rate applications. Another article[18] demonstrates the effectiveness of the Y-shaped slot in achieving tri-band functionality and bandwidth enhancement. The optimised design ensures compact size and good impedance matching, but with the limitation of moderate gain and narrower bandwidth. Immadi *et al.* proposed a tri-band microstrip antenna using geometrical modifications, AI-based algorithms, and resonator structures to enhance bandwidth and

gain. It also explores flexible substrates and advanced fabrication techniques for improved performance[19]. While the design effectively achieves multiband functionality, its larger size may pose limitations for space-constrained applications.

Optimisation of a compact triple-band CPW-fed antenna using geometrical modifications and impedance tuning to enhance bandwidth and radiation efficiency projected in[20]. Behera *et al.* proposed a triple-band settling MPA featuring symmetrical U-slots for WLAN and WIMAX applications. Their design improved resonance and gain response while ensuring adequate air height between the ground plane and radiating patch to enhance bandwidth operation. This study emphasised the growing trend towards multiband antennas capable of supporting multiple communication standards. Raviteja in[21] further contributed to the discourse by analysing the impact of dual trapezoidal slots and partial ground on bandwidth and gain considerations for microstrip antennas. This study illustrated how innovative slot designs can enhance the performance of antenna arrays[22], addressing common limitations such as narrow bandwidth and low gain. The same year, Prasad *et al.*[23] presented a comprehensive review of multiband MPA for various wireless applications, reinforcing the importance of compact and efficient designs in contemporary communication systems. A dual-band metamaterial antenna, emphasising the need for low-profile, cost-effective solutions that maintain high efficiency and stable radiation patterns across multiple frequency bands[24,25]. Benkalfate *et al.*[26] expanded the discourse by discussing the design of Ultra-Wide Band (UWB) MPA operating across a broad frequency range, showcasing the potential for radical modifications to traditional designs to enhance performance. In 5G, MPAs operate in the sub-6 GHz band[27,28] offering expansive bandwidths critical for high-speed data and consistent communication. Ahmad *et al.*[29] introduced a tri-band wearable device for mm-wave 5G applications, emphasising the critical need for high gain[30] and efficiency in compact designs. Zhou *et al.*[31] proposed a meander line-based tri-band microstrip antenna for 5G sub-6 GHz application, provided enhanced bandwidth of 80, 810 and 580 MHz at the three resonant frequencies with peak gain of 3.17, 2.22, and 2.69dBi. Rao *et al.*[32] investigate a compact tri-band omnidirectional antenna for CubeSat application. The suggested antenna delivers 90% radiation efficiency with impedance bandwidth of 80, 250 and 1450 MHz.

This study's objective was to design and examine a compact triple-band antenna for multi-standard services, aiming for enhanced bandwidth characteristics. To accomplish tri-band functionality with adequate bandwidth at each resonant frequency for the intended wireless services, the optimised antenna consists of a circular ring surrounded by a semicircular arch structure, a vertical arrowhead-shaped feeding structure positioned within the ring, and a plano-convex DGP. The suggested antenna provides superior return loss and VSWR, adequate gain, and has a resonant frequency of 2.4, 4.2, and 5.2 with a -10 db impedance bandwidth of 310, 1390, and 290 MHz. As a result, the antenna under investigation is appropriate for WLAN, WIMAX, and 5G services. The paper is organised into several segments. Section 1 provides an introduction, outlining the existing literature and objectives of the research work. Section 2 presents the antenna design conception that includes antenna topology, design evolution mechanism, and parametric analysis of a triple-band MPA. Section 3 exhibits the antenna prototype, followed by the simulated and tested result analysis. Finally, Section 4 concludes the paper with key findings and implications.

2.0 Antenna Design Conception

This section provides a detailed overview of the projected antenna design process that starts with the antenna design topology, followed by the evolution mechanism and the parametric analysis.

2.1 Antenna Topology

The antenna is made up of a circular ring surrounded by the semicircular arch-shaped patch, a vertical arrowhead feeding structure, and a plano-convex-shaped ground plane defected by an equilateral triangle-shaped slot. The projected antenna's structure was powered by a Wf × Lf microstrip transmission line to provide 50Ω port impedance. A low-cost FR4 substrate with a height (h) of 1.59 mm and dielectric constant (εr) of 4.4 is utilised to develop the 36 mm × 25 mm antenna design. The geometrical, top, and rear outlook of the projected antenna design is displayed in Figure 1.

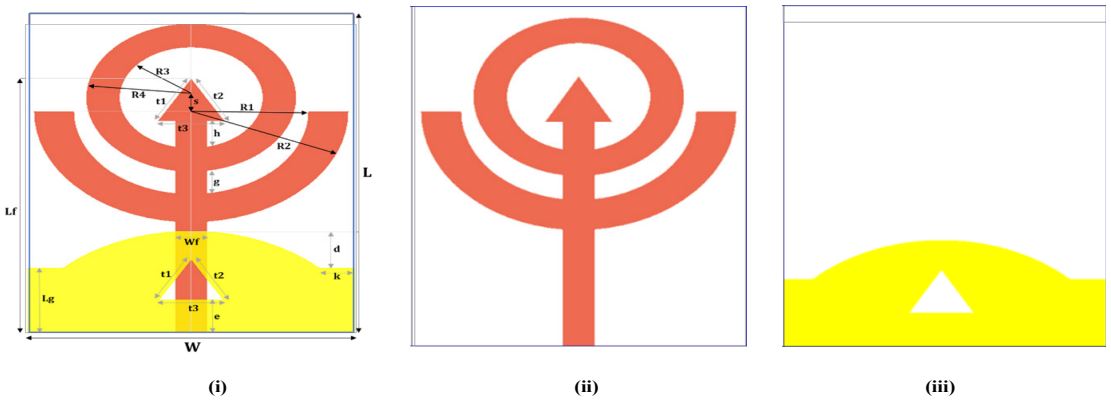


Figure 1. Proposed antenna design structure: **(i)** Geometrical outlook; **(ii)** Top outlook; **(iii)** Rear outlook.

Table 1. Optimised dimension of the projected antenna parameters

Parameters	Size (mm)	Parameters	Size (mm)
L	36	t1	5
W	25	t2	5
Lg	6.9	t3	5
Wf	2.4	d	4
Lf	27.3	e	3.5
R1	9	g	2.3
R2	12	k	2.6
R3	5.5	h	2.6
R4	8	s	1.5

The proposed antenna is said to have the optimised dimensions for integration into compact devices to be utilised for WLAN/WIMAX/5G applications. To attain the optimum performance with tri-band capability, the best-fit parameters of the proposed antenna were determined through the suggested parametric evolution process. Table 1 displays the designed antenna's optimal parameters. The projected antenna's performance was evaluated using the ADS software.

2.2 Antenna Design Evolution Mechanism

To illustrate the antenna's design evolution, Figure 2 presents the step-by-step progression beginning with the basic circular antenna with a finite ground plane to the final proposed design.

The antenna evolution process began with a simple ring-shaped patch that had a partial ground plane. The equation for a circular MPA, specified in Equation (1), was employed to determine the resonant frequency.

For circular patch components, the dominant resonant mode is given by[6]:

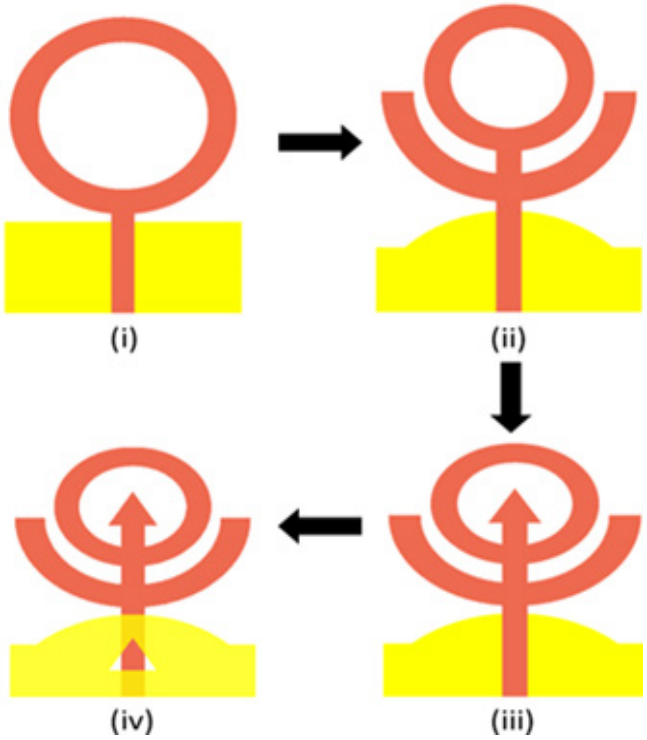


Figure 2. Evolution mechanism of the developed antenna: (i) Stage 1; (ii) Stage 2; (iii) Stage 3; and (iv) developed antenna.

$$f_r = \frac{1.8412c}{2\pi R_{eff}\sqrt{\varepsilon_{eff}}} \quad (1)$$

where R_{eff} Is the effective radius, and it is given by[6]:

$$R_{eff} = R\left(1 + \frac{2h}{\pi R}\left(\ln\left(\frac{\pi R}{2h}\right) + 1.7726\right)\right)^{\frac{1}{2}} \quad (2)$$

where R It is the physical radius of the circular patch. The effective permittivity is given by[4]:

$$\varepsilon_{eff} = \frac{\varepsilon_r + 1}{2} + \frac{\varepsilon_r - 1}{2} \times \left(1 + 12\frac{h}{W}\right)^{-0.5} \quad (3)$$

where ε_r = dielectric constant of the substrate, h = substrate height.

The characteristic impedance of the microstrip feed line is given by[6]:

$$Zo = \frac{120\pi}{\sqrt{\varepsilon_{eff}}}\left(\frac{W}{h} + 1.393 + 0.667\ln\left(\frac{W}{h} + 1.444\right)\right)^{-1} \quad (4)$$

To achieve impedance matching (typically to 50 Ω), the width of the feed line is adjusted. The impedance Band-Width (BW) and Fractional Bandwidth (FBW) of the MPA can be estimated by using Eq. 5 and 6 as given below[4].

$$BW = f_h - f_l \quad (5)$$

$$FBW = \frac{f_h - f_l}{f_0} \times 100\% \quad (6)$$

where f_h, f_l and f_0 Are the upper cutoff, lower cutoff and centre frequencies.

The initial design of the suggested antenna used a simple circular ring-shaped patch with a microstrip feedline construction and finite ground plane as displayed in Figure 2(i). The first stage antenna resonates at two frequencies of 3 GHz and 5.41 GHz, which offers S_{11} of -22.99 and -15.89 db. It featured a -10 db bandwidth of 1585 MHz (2.422-4.007) and 1010 MHz (4.948-5.958).

The finite ground plane utilised in the first phase is changed to a plano-convex form in the second phase, and a semicircular arch-shaped patch is maintained at the outer side of the circular ring. This causes the antenna's centre frequency to shift to the desired 2.4 GHz frequency band with a wider bandwidth in the second frequency band as displayed in Figure 2(ii).

In the third phase, an arrowhead-shaped structure is introduced within the circular patch as depicted in Figure

Table 2. Comparative result analysis for the different phases of the developed antenna

Design Stages	Antenna Parameters			
	Resonance Frequency (GHz)	Return Loss (db)	Operating Bands (GHz)	Bandwidth (MHz)
Stage 1	F_{r1} = 3.00 F_{r2} = 5.41	S_{11} = -22.99 S_{11} = -15.89	2.422-4.007 4.948-5.958	1585 1010
Stage 2	F_{r1} = 2.48 F_{r2} = 4.03	S_{11} = -26.95 S_{11} = -21.46	2.313-2.625 3.444-5292	312 1848
Stage 3	F_{r1} = 2.47 F_{r2} = 4.06 F_{r3} = 5.17	S_{11} = -25.69 S_{11} = -21.37 S_{11} = -27.11	2.297-2.609 3.438-4.984 4.984-5.370	312 1546 386
Stage 4 (Developed Antenna)	F_{r1} = 2.40 F_{r2} = 4.20 F_{r3} = 5.21	S_{11} = -13.59 S_{11} = -29.71 S_{11} = -17.90	2.33-2.64 3.57-4.96 5.08-5.37	310 1390 290

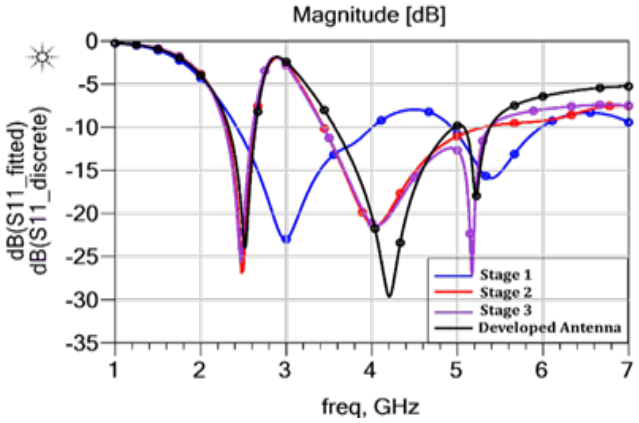


Figure 3. Simulated S_{11} for each stage of the design evolution of the produced antenna.

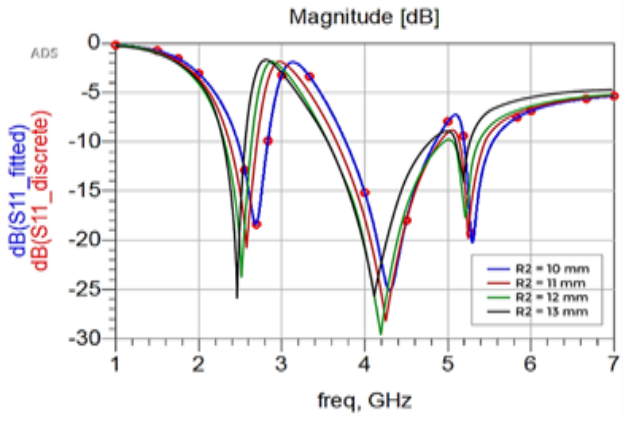


Figure 4. Effect of R2 variations on S_{11} for the produced triple-band antenna.

2(iii). This causes the antenna to start producing the third frequency band, but the S_{11} curve between the 4.2 GHz and 5.2 GHz bands does not rise enough, meaning these bands are not well-isolated. This makes it unclear whether the antenna truly operates as a tri-band antenna or just has an extended second band.

In the last phase of antenna design, the ground plane is defective with an equilateral triangular shape slot. This structure helps to improve the isolation between the 2nd and 3rd frequency bands, and hence we get a more distinct tri-band response as compared to the earlier stage, with adequate bandwidth at all three frequency bands. The final phase of the antenna is revealed in Figure 2(iv) as the optimized design. The simulation results of S_{11} for the different phases of the design evolution of the suggested antenna are displayed in Figure 3.

The different parameters of the developed antenna from stage 1 to the last stage are compared in Table 2 for simpler comprehension.

2.3 Parametric Analysis

We investigated the parametric analysis to fix the resonant frequencies of the 1st, 2nd, and 3rd bands for the intended wireless applications. Initially, we perturb the outer Radius (R2) of the semicircular arch. The radius R2 is decremented from 13 to 10 mm in steps of 1 mm. As displayed in Figure 4, it was observed that this perturbation causes the variation in the 1st and 2nd resonant frequencies. However, very few fluctuations were observed for the 3rd resonant frequency. This helps

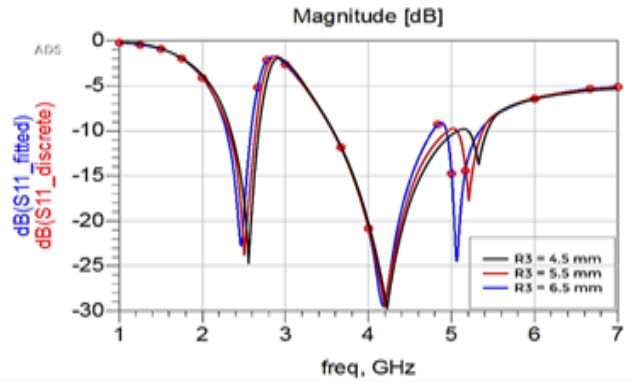


Figure 5. The effect of R3 variations on S_{11} for the produced triple-band antenna.

to fix the 3rd frequency band to 5.08-5.37 GHz. From the results, it is very clear that the best value of S_{11} is attained for R2=12 mm; hence, it is finalised as the optimal value.

In the next stage, we perturb the innermost radius of the circular ring (R3). The radius R3 is incremented from 4.5 to 6.5 mm in steps of 1 mm. As displayed in Figure 5, it was observed that this perturbation causes the variation in the 3rd resonant frequency. However, very little fluctuation was observed for the 1st and 2nd frequency bands. This helps to fix up the 1st and 2nd frequency bands to 2.33-2.64 GHz and 3.57-4.96 GHz, respectively. From the results, it is very clear that the best value of S_{11} is attained for R3=5.5 mm; hence, it is finalised as the optimal value.

Thus, we inferred that the resonant modes of the designed antenna were highly influenced by variations

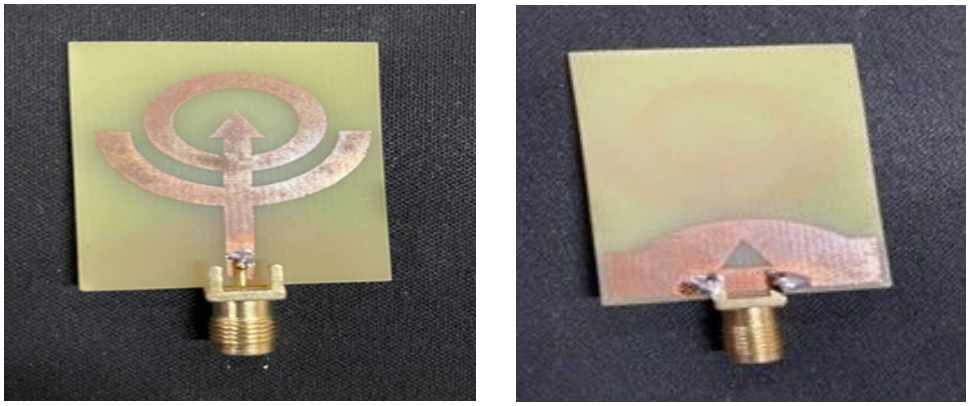
in the parameters R2 and R3. To attain the optimum performance with triple-band capability, the best-fit parameters of the projected antenna were determined through the suggested parametric evolution process. Table 2.1 displays the designed antenna's optimal parameters.

3.0 Experimental Results and Discussion

This segment unveils simulation and measurement results to illustrate the performance of the suggested antenna. The fabricated antenna's prototype design, displayed in Figure 6, presents the top view of the radiating patch and the ground plane. The fabricated antenna is tested by utilising the Vector Network Analyser (VNA) to compare simulated results with the measured ones.

3.1 Return Loss and VSWR

The return loss (S_{11}) measures the amount of power reflected from the antenna compared to the incident power. The simulated and measured S_{11} for the aforementioned triple-band frequencies are -13.593, -29.705, -17.901 db, and -12.593, -24.705, -16.901 db, respectively. This indicates the antenna is reflecting the least amount of power to the source input port. The simulated and measured values of S11 are portrayed in Figure 7.



(i) **(ii)**

Figure 6. Fabricated design of a proposed triple-band antenna: **(i)** Top view of radiating patch; **(ii)** Ground plane.

Table 3. Comparison between the simulated result and the measured result

Results	Antenna Parameters			
	Resonating Frequency (Fr in GHz)	**Return Loss (S_{11} in db)**	**VSWR**	**Bandwidth (MHz)**
Simulated (ADS)	2.406	-13.593	1.529	310
	4.204	-29.705	1.068	1390
	5.212	-17.901	1.292	290
Measured (VNA)	2.406	-12.593	1.829	280
	4.204	-24.705	1.468	1200
	5.212	-16.901	1.892	210

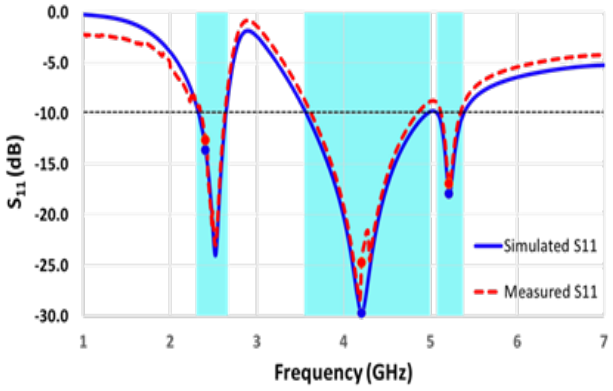


Figure 7. Simulated and measured S11 of the proposed triple-band antenna.

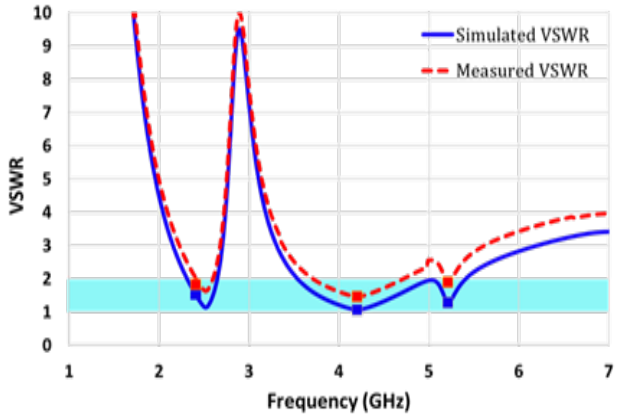


Figure 8. Simulated and measured VSWR of the proposed triple-band Antenna on VNA.

The S_{11} values obtained from VNA measurements show a reasonable correlation with simulated results. The measured values are slightly different from the simulated values, indicating a marginal degradation in impedance matching, possibly due to fabrication imperfections or connector losses. The measurements of the designed antenna will reveal triple frequency bands with -10 dB impedance bandwidths of 310 MHz (2.33-2.64 GHz), 1390 MHz (3.57-4.96 GHz), and 290 MHz (5.08-5.37 GHz), which make it useful for applications such as WLAN (2.4/5.2 GHz), WIMAX (2.5/3.5 GHz), and 5G NR Sub-6 GHz band (3.3–4.2 GHz n78 band & 4.4–5.0 GHz n79 band).

The Voltage Standing Wave Ratio indicates the extent of impedance match between the antenna and the transmission line. A VSWR between 1 ≤ VSWR ≤ 2 is considered good, meaning minimal signal reflections. The simulated and measured VSWR of the projected antenna at 2.4, 4.2, and 5.2 GHz are 1.529, 1.068, 1.292, and 1.829, 1.468, and 1.892, respectively. The obtained results, as displayed in Figure 8, clearly indicate a good impedance matching, which meets the desired objective. The minor difference between the measured VSWR values and the simulated ones suggests slight impedance mismatches in practical implementation.

Table 3 compares the simulated and the measured outcomes of S_{11}, VSWR, and operating bandwidth. The minor variations in simulated and measured results are possibly due to fabrication imperfections or connector losses.

3.2 Gain

Gain (G) represents the actual power radiated in a given direction. High gain signifies better radiation performance. Figure 9 below displays the simulated Gain plot of the projected antenna structure. As revealed in Figure 9, the gain of the antenna is found to be 2.92, 3.76, and 4.24 dBi at 2.4, 4.2, and 5.2 GHz, respectively. The peak gain achieved by the antenna is in the second frequency band, and it is found to be 5.78 dBi. As a result, the projected antenna is less susceptible to fading and interference.

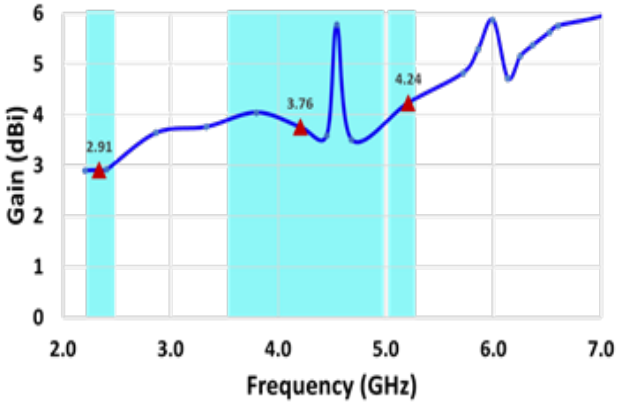


Figure 9. Simulated gain plot for the designed antenna.

3.3 Efficiency

An important metric that measures how well an antenna transforms electrical power supplied into electromagnetic energy that is radiated is antenna efficiency. It is

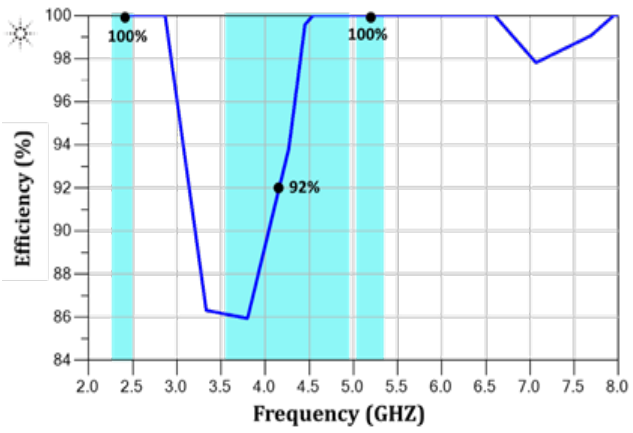


Figure 10. Simulated Efficiency plot for the designed antenna.

defined as the ratio of the radiated power to the total input power, which includes impedance mismatches, conduction losses, and losses from dielectric materials. At the resonant frequencies of 2.4, 4.2, and 5.2 GHz, the efficiency of the proposed tri-band antenna design is 100%, 92%, and 100%, as shown in Figure 10. These findings show that the antenna operates best at the appropriate resonant frequencies. Effective impedance matching and low resistive losses throughout the working bands are suggested by this result.

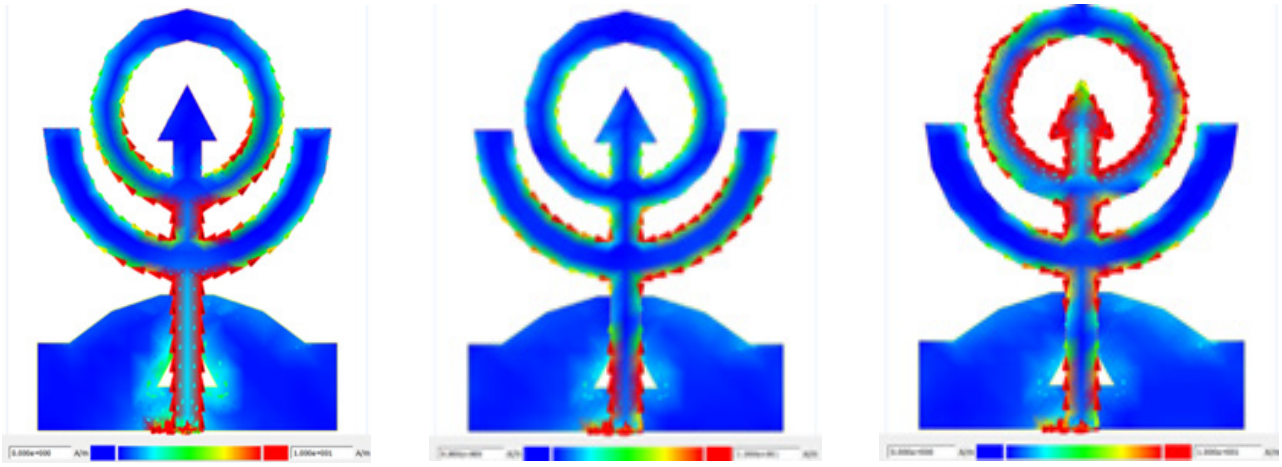
3.4 Surface Current Distribution

The surface current distribution analysis of the projected antenna at different frequencies reveals its multiband behaviour. Figure 11(i) reveals that at 2.4 GHz, the current is concentrated along the feedline and lower circular patch, indicating fundamental mode excitation. At 4.2 GHz, the current shifts towards the middle and upper sections, showing higher-order mode excitation displayed in Figure 11(ii). At 5.2 GHz, the current is more evenly distributed across the entire structure, especially along the circular ring and top elements illustrated in Figure 11(iii). This progression confirms that different segments of the antenna contribute to resonance at different frequencies. The observed mode shifting enhances impedance matching and radiation efficiency, making antenna fitting for triple-band operation.

3.5 Radiation Pattern

The directionality of an antenna's radio frequency signal power is explained by a radiation pattern. It displays the spatial distribution of the radiated energy in the intended direction schematically.

The simulated radiation patterns in the E- and H-planes at 2.4, 4.2, and 5.2 GHz are displayed in Figure 12. The antenna exhibits an omnidirectional pattern at 2.4 GHz, ensuring uniform radiation coverage. At 4.2 GHz, slight distortions appear in the E-plane, indicating the presence of higher-order modes, while the H-plane pattern remains stable. At 5.2 GHz, the radiation pattern further evolves, showing more directivity in the E-plane. The antenna maintains good radiation efficiency across all frequencies, but minor variations at higher bands suggest a



(i) (ii) (iii)

Figure 11. Surface current distribution at centred frequencies: (i) 2.4 GHz; (ii) 4.2 GHz; and (iii) 5.2 GHz.

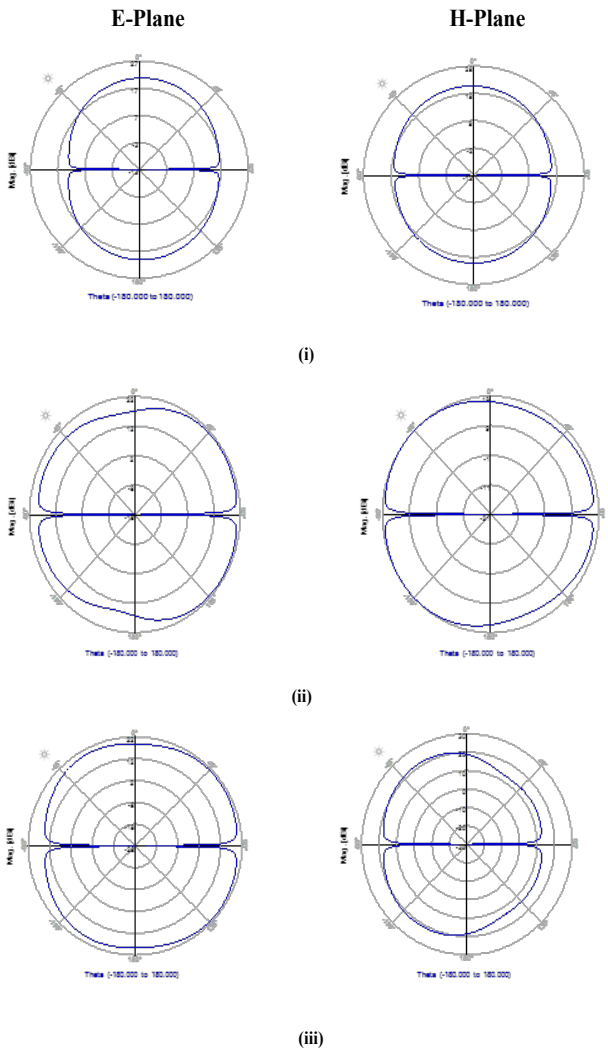


Figure 12. Radiation patterns of the designed antenna in the E-plane and H-plane at **(i)** 2.4 GHz, **(ii)** 4.2 GHz, **(iii)** 5.2 GHz.

trade-off between omnidirectionality and directivity. The stable H-plane radiation ensures consistent performance by the antenna and makes it suitable for WLAN, WIMAX, and 5G applications.

3.6 Co-polar and Cross-Polar Radiation Pattern

The developed antenna structure's simulated co-polar and cross-polar radiation patterns at 2.4, 4.2, and 5.2 GHz in E-Plane and H-Plane are displayed in Figure 13. In the E-plane, Etheta and Ephi represent the co-polar and cross-polar components, respectively, whereas in the

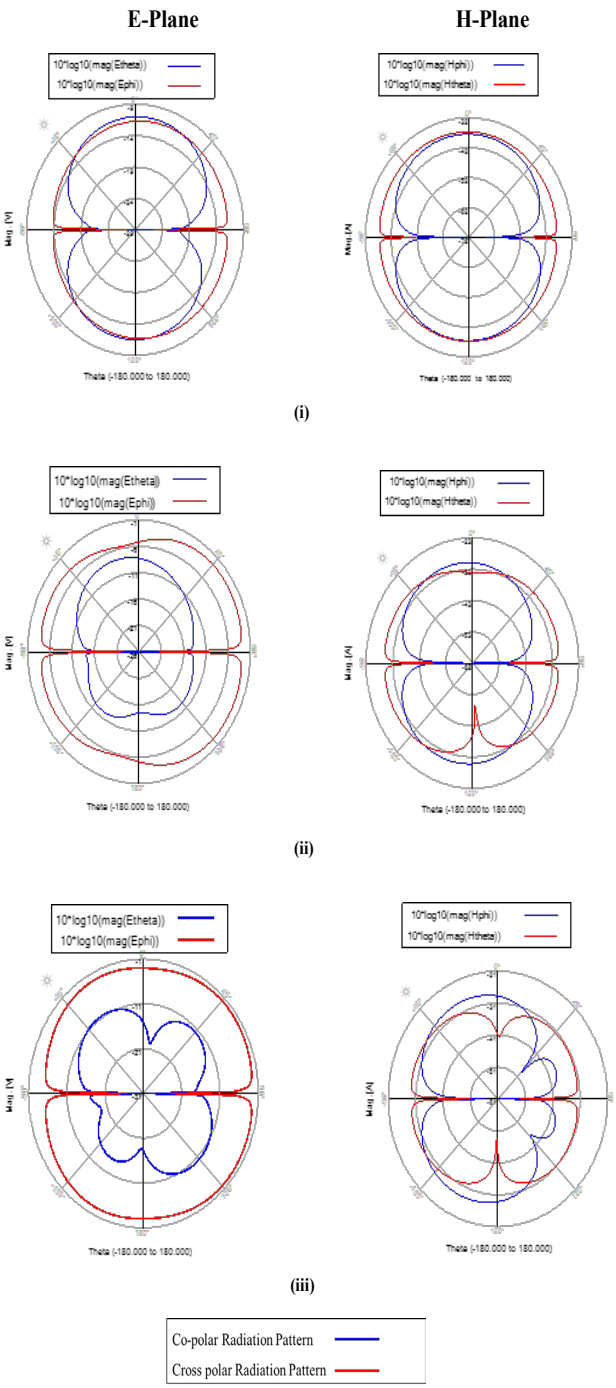


Figure 13. Designed antenna's co-polar and cross-polar radiation patterns in E-plane and H-plane at **(i)** 2.4GHz; **(ii)** 4.2GHz; **(iii)** 5.2GHz.

H-plane, Hphi and Htheta denote the co-polar and cross-polar components. At 2.4 GHz, the co-polar component

Table 4. Performance comparison with the existing earlier antennas

Reference	Antenna Type	Material Used	Resonant Frequency (GHz)	Operating Band (GHz)	Bandwidth (MHz)	Return Loss (db)	Gain (dBi)	Size (mm^2)	Applications
11	MPA Loaded with Notches and Slots	FR4	1.422 1.791 2.467	1.409–1.437 1.723–1.911 2.045–2.858	28 188 813	-18.18 -12.78 -34.52	3.287 3.067 3.480	38.04 × 29.44	L Band Bluetooth
14	F-shaped Planar patch	FR4	1.8 3.5 5.4	1.74–1.88 3.42-3,6 5.34-5.54	140 180 200	-14 -16 -18	2.34 5.2 1.42	60 × 50	DCS / WLAN / WIMAX
17	Meander line structured Patch	FR4	0.9 1.8 2.4	0.88-0.91 1.79-1.83 2.39-2.42	30 40 30	-33 -46 -24	1.62 2.12 1.89	42 × 15	GSM/DCS/ WLAN
18	Y-shaped patch with DGS	FR4	4 4.9 5.5	3.829-4.185 4.691-5.134 5.330-5.618	356 443 287	-18.82 -19.91 -25.25	2.69 7.27 1.37	50.5 × 41.12	5G wireless communication
19	MIMO antenna with SRR	FR4	3 4.1 5.2	4.11–4.13 5.18–5.21 3.04–3.09	20 30 50	−20.06 −19.16 −22.07	2.5	60 × 60	5G wireless communication
20	CPW-fed Spider-wave hexagonal-shaped Patch	FR4	3.27 5.89 8.27	3.17–3.48 5.51–6.28 8.11–8.52	310 770 410	-28 -25 -23	2.99 4.14 1.62	35 × 30	5G mid-band cellular networks/ Wi-Fi 6
Proposed antenna	Circular ring with arch-shaped patch and DGS	FR4	2.4 4.2 5.2	2.33–2.64 3.57–4.96 5.08–5.37	310 1390 290	-13.59 -29.70 -17.90	2.92 3.76 4.24	36 × 25	WLAN / WIMAX / 5G NR band

exhibits a well-defined main lobe with minimal cross-polarisation, indicating good polarisation purity. At 4.2 GHz, the radiation pattern remains stable, but cross-polarisation slightly increases due to higher-order modes or structural asymmetries. At 5.2 GHz, the co-polar pattern becomes slightly distorted, and cross-polarisation increases further, possibly due to fabrication tolerances or edge diffraction effects. Overall, the antenna maintains good polarisation performance, but higher frequencies introduce slight degradation in cross-polarisation levels.

Table 4 highlights the performance comparison of the suggested antenna with the existing antennas described in the literature. The comparison is made concerning antennas' lower, mid, and upper resonant frequency bands to validate the projected antenna design for the desired wireless applications.

The projected antenna demonstrates superior multiband performance compared to earlier designs, covering WLAN, WIMAX, and 5G NR bands effectively. It achieves wider bandwidths of 310 MHz at 2.4 GHz, 1390 MHz at 4.2 GHz, and 290 MHz at 5.2 GHz, surpassing many existing designs for WLAN/WIMAX applications, while maintaining a compact size of 36 × 25 mm². The gain values (2.92 dBi at 2.4 GHz, 3.76 dBi at 4.2 GHz, and 4.24 dBi at 5.2 GHz) are competitive with previous works, ensuring good radiation efficiency. Additionally, its return loss performance (-13.59 db to -29.70 db) indicates effective impedance matching across the operating bands. The integration of a circular ring with an arch-shaped patch, arrowhead feed, and DGP enhances multiband operation, making it a strong contender for modern wireless communication applications.

4.0 Conclusion

A novel multiband MPA efficiently operates at triple band, making it suitable for WLAN/WIMAX/5G applications. Three resonating modes with good impedance characteristics are attained by incorporating a semicircular arch-shaped structure, a vertical arrowhead-shaped feed, and a plano-convex DGP. The projected antenna exhibits miniaturisation with excellent return loss and VSWR, a wider bandwidth of 1.39 GHz at the mid-frequency band, acceptable gain, and radiation characteristics. The impact of altering the sizes of critical design parameters on the antenna performance parameters leads to optimised performance and a compact size of 36×25 mm². Overall, the designed antenna offers a balance between multiband functionality, compact size, and uniform radiation characteristics, rendering it a viable option for contemporary wireless communication systems. The design can be extended by implementing it on flexible or textile substrates to explore its performance under bending, for wearable or biomedical applications.

5.0 References

1. Kumar H, Srivastava S. Rectangular and circular antenna design on thick substrate. J Telecom. 2010; 2. https://doi.org/10.48550/arXiv.1006.0836
2. Binaya S, Barad D, Behera S. A triple-band suspended microstrip antenna with symmetrical U-slots for WLAN/WIMAX applications. Adv Electromagn. 2018; 7(2). https://doi.org/10.7716/aem.v7i2.608
3. Chhaule N, Koley C, Mandal S, Onen A, Ustun TS. A comprehensive review on conventional and machine learning-assisted design of 5G microstrip patch antenna. Electronics. 2024; 13(19). https://doi.org/10.3390/electronics13193819
4. Balanis CA. Antenna theory: analysis and design. 4th ed. Hoboken, NJ: Wiley; 2016.
5. Kedze KE, Wang H, Park YB, Park I. Substrate dielectric constant effects on the performances of a metasurface-based circularly polarized microstrip patch antenna. Int J Antennas Propag. 2022; 2022. https://doi.org/10.1155/2022/3026677
6. Pozar DM. Microwave engineering. 4th ed. Hoboken, NJ: Wiley; 2011.
7. Iqbal J, Illahi U, Yasin MNM, Albreem MA, Akbar MF. Bandwidth enhancement by using a parasitic patch on a dielectric resonator antenna for sub-6 GHz 5G NR bands application. Alex Eng J. 2022; 61(6):5021-32. https://doi.org/10.1016/j.aej.2021.09.049
8. Malfajani RS, Ashraf FB, Sharawi MS. A 5G enabled shared-aperture, dual-band, in-rim antenna system for wireless handsets. IEEE Open J Antennas Propag. 2022; 3:1013-24. https://doi.org/10.1109/OJAP.2022.3201627
9. Kahina D, Mouloud C, Mokrane D, Faiza M, Rabia A. A compact ACS-fed tri-band microstrip monopole antenna for WLAN/WiMAX applications. Adv Electromagn. 2018; 7(5). https://doi.org/10.7716/aem.v7i5.853
10. Huang HF, Zhang SF. Compact multiband monopole antenna for WLAN/WiMAX applications. Microw

Opt Technol Lett. 2014; 56(8):1809-12. https://doi.org/10.1002/mop.28452
11. Verma RK, Srivastava DK. Design and analysis of triple-band rectangular microstrip antenna loaded with notches and slots for wireless applications. Wirel Pers Commun. 2020; 114(2):1847-64. https://doi.org/10.1007/s11277-020-07452-6
12. Naidu VP, Kumar R. Design of compact dual-band/tri-band CPW-fed monopole antennas for WLAN/WiMAX applications. Wirel Pers Commun. 2015; 82(1):267-82. https://doi.org/10.1007/s11277-014-2207-z
13. Murugesh M, Lim EH, Chee PS, Bong FL. Polarisation-insensitive planar patch antenna with large embedded serial capacitance for on-metal tag design. Sci Rep. 2023; 13(1). https://doi.org/10.1038/s41598-023-34836-y
14. Elkorany AS, Mousa AN, Ahmad S, Saleeb DA, Ghaffar A, Soruri M, *et al*. Implementation of a miniaturised planar tri-band microstrip patch antenna for wireless sensors in mobile applications. Sensors. 2022; 22(2). https://doi.org/10.3390/s22020667
15. Karthikeyan M, Sitharthan R, Ali T, Pathan S, Anguera J, Shanmuga Sundar D. Stacked T-shaped strips compact antenna for WLAN and WIMAX applications. Wirel Pers Commun. 2022; 123(2):1523-36. https://doi.org/10.1007/s11277-021-09198-1
16. Li L, Zhang X, Yin X, Zhou L. A compact triple-band printed monopole antenna for WLAN/WIMAX applications. IEEE Antennas Wirel Propag Lett. 2016; 15:1853-5. https://doi.org/10.1109/LAWP.2016.2539358
17. Sun X. Design of a triple-band antenna based on its current distribution. Prog Electromagn Res Lett. 2020; 90. https://doi.org/10.2528/PIERL19122502
18. Singh A, Joshi S. Design of Y-shaped tri-band rectangular slot DGS patch antenna at sub-6 GHz frequency range for 5G communication. J Eng Appl Sci. 2024; 71(1). https://doi.org/10.1186/s44147-024-00476-w
19. Immadi G, Narayana MV, Navya A, Madhuri AS, Krishna BV, Gopi MVS. Analysis of a triple band MIMO antenna for sub-6 GHz applications. Prog Electromagn Res B. 2024; 107:47-62. https://doi.org/10.2528/PIERB24032802
20. Singh SK, Banda YD, Kumar M, Yadav AK, Singh HM, Yahya MZA, *et al*. A compact triple-band CPW-fed antenna laminated on FR-4 dielectric substrate material for diverse wireless applications. Curr Appl Phys. 2025; 71:27-36. https://doi.org/10.1016/j.cap.2024.12.002
21. Raviteja GV. An insight into the impact of partial ground and dual trapezoidal slots on bandwidth and gain considerations for a microstrip antenna array for WIMAX application. Adv Electromagn. 2018; 7(5). https://doi.org/10.7716/aem.v7i5.772
22. Awais M, Madni A, Khan WT. Design of a compact high-isolation 4-element wideband patch antenna array for GNSS applications. IEEE Access. 2022; 10:13780-6. https://doi.org/10.1109/ACCESS.2022.3147600
23. Prasad L, Ramesh B, Kumar KSR, Vinay KP. Design and implementation of multiband microstrip patch antenna for wireless applications. Adv Electromagn. 2018; 7(3). https://doi.org/10.7716/aem.v7i3.646
24. Milias C, Andersen RB, Lazaridis PI, Zaharis ZD, Muhammad B, Kristensen JTB, *et al*. Miniaturised multiband metamaterial antennas with dual-band isolation enhancement. IEEE Access. 2022; 10:64952-64. https://doi.org/10.1109/ACCESS.2022.3183800
25. Hasan MM, Faruque MRI, Islam MT. Dual-band metamaterial antenna for LTE/Bluetooth/WiMAX system. Sci Rep. 2018; 8(1). https://doi.org/10.1038/s41598-018-19705-3
26. Benkalfate C, Feham M, Ouslimani A, Kasbari A. UWB patch antenna design and realisation in the bandwidth 780MHz to 4.22GHz. In: Conference on Electrical Engineering; 2019. https://arxiv.org/abs/2207.00152
27. Nahar T, Rawat S, Pathak P, Kumar P, Anguera J. Leaf-shaped antennas for sub-6 GHz 5G applications. IEEE Access. 2024; 12:114338-57. https://doi.org/10.1109/ACCESS.2024.3435528
28. Padmanathan S, Abdullah Al-Hadi A, Elshirkasi AM, Al-Bawri SS, Islam MT, Sabapathy T, *et al*. Compact multiband reconfigurable MIMO antenna for sub-6GHz 5G mobile terminal. IEEE Access. 2022; 10:60241-52. https://doi.org/10.1109/ACCESS.2022.3180048
29. Ahmad S, Boubakar H, Naseer S, Alim ME, Sheikh YA, Ghaffar A, *et al*. Design of a tri-band wearable antenna for millimetre-wave 5G applications. Sensors. 2022; 22(20). https://doi.org/10.3390/s22208012
30. Paracha KN, Rahim SKA, Soh PJ, Kamarudin MR, Tan KG, Lo YC, *et al*. A low profile, dual-band, dual polarised antenna for indoor/outdoor wearable application. IEEE Access. 2019; 7:33277-88. https://doi.org/10.1109/ACCESS.2019.2894330
31. Zhou JF, Li JS. A meander line integrated rectangular tri-band antenna for 5G sub-6GHz applications. Microw Opt Technol Lett. 2025. https://doi.org/10.1002/mop.70164
32. Rao S, Slawomir K, Anna P. A compact tri-band omnidirectional antenna design for CubeSat applications. Sci Rep. 2025; 15:11908. https://doi.org/10.1038/s41598-025-96628-w